Application of Wind Profiles from UV Lidar in Nowcasting for Mauna Kea Observatories

S. Businger[1], I. Dors[2], S. Turco[2], J. McHugh[2], J. Ryan[2], T. Cherubini[1],
J. B. Moore[2], C, Nardell[3], and P. Hays[3]
[1]University of Hawaii, [2]University of New Hampshire, [3]Michigan Aerospace Corporation

ABSTRACT

The recently commissioned GroundWinds Lidar Observatory, based at ~3300 m on the slope of Mauna Loa, can measure altitude resolved line-of-sight wind velocities, turbulence power spectra, aerosol content and faint cirrus clouds among other things of interest to astronomers. The overarching goal of the GroundWinds program is to develop and demonstrate incoherent ultra-violet lidar technology for a future space-based system that will measure the vertical structure of global winds from molecular backscatter. The lidar observatory employs spectral line profiling of incoherent backscattered 355 nm laser light. Very rapid measurement of the Doppler shift (400 ns resolution) is accomplished by feeding the returned laser light into a combination of two Fabry-Perot etalons and collapsing the interference fringes into a 1-dimensional interference pattern using a conical optic. This allows the system to get the maximum signal to noise ratio and best vertical resolution given the performance of the CCD. Each measurement takes 10 s. The molecular return is strong up to 15-km altitude. The YAG laser is pulsed at 10 Hz, and each pulse is stretched to 50 ns; the average power dissipated is 5 W. The outgoing beam is expanded to match the field of view of the telescope. The Doppler shift as a function of altitude, measured along two lines of sight orthogonal to one another, is then used to determine the horizontal wind velocity as a function of altitude. The incoherent lidar system can operate day or night. In addition, the lidar can be operated with a very short integration time and used to directly measure turbulence spectra over a range of elevations. A recent intercomparison campaign has demonstrated the accuracy of the GroundWinds instrument. In addition to average wind measurements intended for global winds, the lidar can be operated with a very short integration time and used to directly measure turbulence spectra over a range of elevations. The turbulence spectra are used to approximate the velocity turbulence parameter, c_v^2, and turbulent dissipation. A recent comparison with an independent measurement of c_T^2 has shown good agreement. Data from the incoherent lidar are used in a custom forecasting project (Mauna Kea Weather Center: http://hokukea.soest.hawaii.edu) that provides operational support for the world-class group of astronomical observatories located on the summit of Mauna Kea. The lidar data are used to help prepare wind and turbulence nowcasts/forecasts for the summit of Mauna Kea (~4000 m) and as input for an operational mesoscale numerical weather prediction model (MM5). Clear-air turbulence in both the free atmosphere and in the summit boundary layer causes phase distortions to incoming electromagnetic wave fronts, resulting in motion, intensity fluctuations (scintillation), and blurring of images obtained by ground-based telescopes. Astronomical parameters that quantify these effects are generically referred to as *seeing*. Seeing improves or degrades with changes in the vertical location and strength of turbulence as quantified by profiles of the refractive index structure function c_n^2. c_n^2 fluctuations usually occur at scales that are too small for routine direct measurement, but they can be parameterized from vertical gradients in wind, temperature, and moisture in our MM5 runs. Seeing at a particular wavelength is then calculated by vertically integrating the c_n^2 profile. Lidar wind profiles represent an important data resource for nowcasting seeing, input for MM5 initial conditions and algorithm refinement, and for forecast verification.

Keywords: direct detection, LIDAR, GroundWinds, Doppler, Fabry-Perot, seeing, turbulence, forecasting

1. INTRODUCTION

INSTRUMENT

1.1 Overview

The GroundWinds instrument on the north slope of Mauna Loa is now measuring line-of-sight wind velocities and other quantities of interest to astronomers. Its original purpose is to be a demonstration for adapting similar technology in space to measure global winds that can improve weather forecasts. However, it also serves as a stand-alone scientific facility that can produce data products such as turbulence power spectra that are of interest to the astromonical community. As a lidar observatory it emits a pulsed beam of 355 nm laser light. Air and aerosols scatter this light, some of which returns to the observatory and, as a function of altitude, is analyzed spectroscopically. From this spectrum one can measure several physical properties of the atmosphere. The incoherent lidar system used here employs a Fabry-Pérot interferometer as a high spectral resolution element, capable of detecting Doppler shifts of the backscattered signal that correspond to velocities less than 1 $m\text{-}s^{-1}$.

The analyzable signal consists of two distinct and superposed components. There is a broad return caused by Rayleigh scattering from atmospheric gases, and a narrow return from Mie scattering from aerosols. The GroundWinds system uses both of these components to measure wind velocity. The aerosol component, when present, allows for accurate wind measurement (< 1 $m\text{-}s^{-1}$), but at high altitudes on Hawaii aerosols are often not present. The molecular component, however, is always present, and is the primary source used to measure wind. Each of these components is measured using an interferometer with a resolution optimized for that measurement.

The key elements of GroundWinds are: a) the interferometer, b) the laser, c) the transmitting telescope, d) the receiving telescope, and e) an instrument control and data processing system. The following discussion describes the instrument beginning with the outgoing laser beam and progressing through to the detectors. This system is also illustrated in a more schematic form in Figure 2.

The 355 nm laser beam exits the instrument through a beam expander that reduces the divergence angle of the emerging light. The narrow transmitted beam allows the receiving telescope to use a small field of view to minimize the system etendue, reduce the size of detection optical system, and minimize stray light transmitted to the detectors. The laser light beam is scattered by the molecules and aerosols in the atmosphere resulting in a detectable backscatter signal. This backscattered light is collected by the primary receiving telescope that tracks the laser beam as the laser beam expander and telescope are rotated in azimuth to observe different horizontal components of the wind. The telescope with an active alignment system focuses the light onto a fiber optic. The fiber optic cable carries the scattered light from the main receiving telescope to the interferometer subsystem. In the meantime, the outgoing light signal is introduced into the primary optical chain through a mirror system. This allows a small fraction of outgoing light from the laser beam to be used as a wavelength reference. The backscattered light and the reference beam are then passed through a narrow-band filter system composed of a dielectric filter and a low resolution Fabry-Pérot etalon. After filtering, the light is introduced into the molecular interferometer and the resulting spectrum is focused into the patented Circle to Line Interferometer Optical system (CLIO). This device converts the circular fringes from the Fabry-Pérot into a linear pattern that is detected with a charge-coupled device (CCD). The circular fringe pattern created by the molecular etalon is present in the transmitted light. The reflected light from the etalon is the complement of the transmitted fringe pattern. In most interferometers, the reflected light is lost from the system. However, in the GroundWinds interferometer the reflected light from the molecular etalon is transmitted into the aerosol etalon via a fiber optic. Here again the etalon creates a velocity sensitive circular fringe pattern that is transformed into a linear pattern by a CLIO, that is in turn coupled to a CCD camera. The light that is not transmitted through either etalon illuminates a photomultiplier tube (PMT). The PMT measures the photometric return as a function of altitude. These data can be used as a measure of the integrated energy returned, and have value in evaluating any misalignment in the etalons. The system detectors record at any one time three sets of information; 1) the aerosol fringe pattern optimized to detect the motion of aerosols, 2) the molecular direct fringe pattern, optimized to detect the motion of the molecular component of the atmosphere, and 3) the integrated photometric return. Unlike other LIDARs, this system utilizes a unique CCD imaging technology to determine simultaneously the range and spectrum of the backscattered light. There are several advantages of using CCD's as the primary detectors as described below.

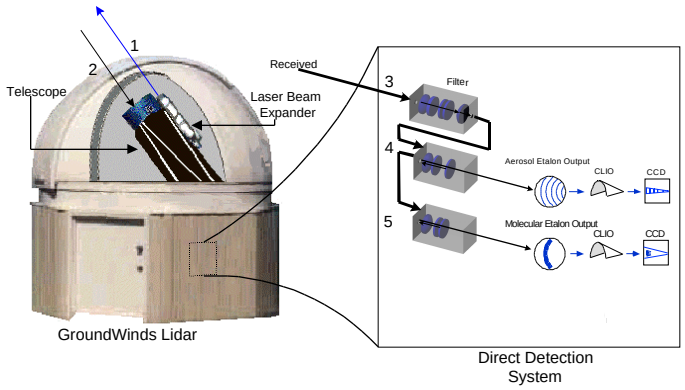

Figure 2: A depiction of the entire optical system.

1.2 Instrument Details

1.2.1 Interferometer

In order to explain how this system works, we must examine the operation of a Fabry-Pérot interferometer. The Fabry-Pérot is often touted as an efficient user of light, and in some respects this is true (Jacquinot, 1954). However, the device actually discards a significant fraction of the incident light. If one order of an interferometer with plate reflectivity R is projected onto a detector, a fraction $(1–R)/(1+R)$ of the light incident on the etalon is actually transmitted while the remainder is reflected. This reflected light amounts to a fraction $2R/(1+R)$. For example, if R=0.90 then 95% of the light is reflected. If less than a full free spectral range is projected on the detector, then a somewhat higher fraction of the light is transmitted. In an effort to keep the size of the instrument to a minimum some studies of incoherent lidar have projected less than a full free spectral range on the detector (Hays et al., 1984; Rees and McDermid, 1990).

1.2.2 CLIO

The Fabry-Pérot interference pattern for a conventional interferometer appears as a set of concentric rings at the infinity focus of the interferometer objective lens, where the detector system is located. The left portion of figure 7 shows this interference pattern as it would appear in the image plane of a conventional instrument. A technique for converting the circular fringes of a Fabry-Pérot interferometer into a linear pattern which can be detected with a conventional linear detector has been described by Hays (1990). The technique, called the Circle to Line Interferometer Optical system (CLIO, U.S. Patent #4,893,003), simplifies the analysis of interferometric information by converting the circular rings, or fringes, into a linear pattern similar to that produced by a conventional spectrometer.

The specific optical technique used to produce this linear interference pattern is to transform the rings that appear at the infinite focus of the objective lens in a Fabry-Pérot interferometer into a series of line segments on the axis of a 45° half-angle internally reflecting cone. In practice the transformation may be accomplished using a 90° sector of a cone to transform a 90° sector of the circular ring pattern on to the cone axis.

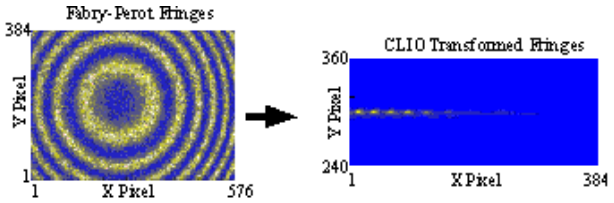

Figure 7: Transformation of Fabry-Perot fringes performed by CLIO

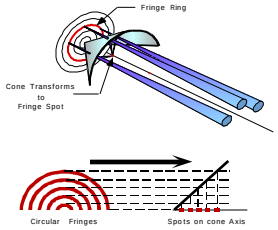

Figure 8: Conceptual ray trace showing the CLIO concept

Light Recycling The GroundWinds instrument measures both molecular and aerosol backscatter with two separate and independent detectors. The light from each laser pulse in the GroundWinds instrument serves both channels. This was only possible through the development of a light recycler that utilizes the reflected light from the etalon plates of the molecular channel to feed the aerosol channel. This innovation is significant because it allows the simultaneous determination of Doppler shifts from Mie scattering as well as Rayleigh. We refer to this as light recycling (U.S. patent #6,163,380), and can be used not only as a way of injecting the signal into two interferometers, but also as a means of reintroducing the signal into a channel multiple times to improve the throughput of a single channel.

The implementation of this idea is accomplished through the use of fiber optic arrays. These arrays use a single multimode fiber optic to introduce the light into the interferometer off-axis. The rejected light appears at the symmetrical point on the other side of the optical axis. If a fiber optic is positioned at the point where this rejected light is in focus, it can be collected and reintroduced at a point on the same side of the axis where it was initially injected. This can be done several times to force as much light as possible through the instrument. It should be noted that the fiber optic has the unique and important property of eliminating spatial coherence while maintaining spectral coherence. This is the essence of the direct detection technique. One might think that a mirror could be used for this recycling technique, but in fact, a mirror would not be effective, because the spatial coherence must be destroyed in order to yield significant throughput on subsequent recycling.

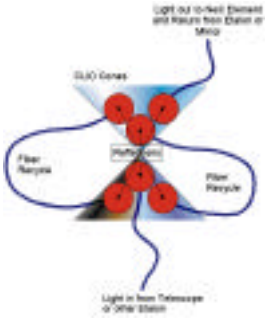

Figure 9: Schematic of the fiber optic ferule used for light recycling.

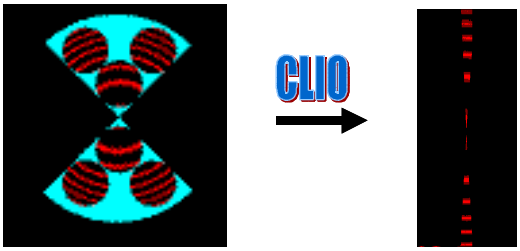

Figure 10: The left figure shows how the Fabry-Perot ring pattern is illuminated with the fiber optic recycler. The relative intensity is not shown to scale. The figure on the right shows the ring pattern after it has been optically transformed by the CLIO optic on the detector.

Telescope The telescope subsystem consists of one transmitter telescope and one receiver telescope. The telescopes with parallel axes are mounted together on a common gimbal that has an azimth range of 290˚ but is fixed in elevation at 45˚.

Laser The GroundWinds system uses a commercial Nd:YAG laser. A custom Continuum 8010 laser was chosen for this system. The laser provides ~4 watts of output power at 355 nm, seeded for a single frequency output. The pulse length of this laser was chosen to be somewhat longer than was actually required, i.e., 50 ns. The laser is fired at a repetition rate of 10 Hz.

Detector During the time following a firing of the laser, the photons received by the telescope and processed through the interferometers, are deposited by the CLIO on a narrow wedge region in the center of the CCD. This wedge of light is a few pixels wide and extends over the entire length of the device (figure 11). The spectrum of the returning light is dispersed along this wedge. In order to separate individual ranges the charge in this narrow wedge on the CCD is electronically translated through the chip during the signal return period. This results in a matrix of charge being deposited in the individual potential wells of the CCD after the return of a single laser light pulse.

While the CCD is shifting the pixels upward, a very small portion of the laser light is leaked into the interferometer and onto the CCD. This provides the laser spectral reference. As the laser pulse propagates through the atmosphere, the CCD chip is continually shifting data upward so as to save the image data from previous altitudes and expose new pixels. In this way, an image is created, with each row of pixels containing spectral information at a particular altitude. Once the entire return signal is collected, the CCD resets to the bottom and waits for the next return signal from the atmosphere. In this manner, multiple shots may be accumulated on chip, so that the signal to noise may be maximized by not incurring a read noise penalty by reading out more often.

3. DATA

The data of interest to the astrophysical community derive from the moments of the line profile of the various fringes primarily in the molecular channel. The amplitude of the signal in the aerosol channel relative to that in the molecular channel is a sensitive indicator of clouds. The first moment of the line profile in the molecular channel yields the line-of-sight air velocity and as discussed below the variation in this LOS wind velocity can be used to estimate the turbulence power spectrum for any altitude. Shown in the accompanying figures (taken from a sister facility in New Hampshire operating at 532 nm) are wind velocities measured by both channels (gray scale) for different altitudes (vertical scale) as a function of time (horizontal scale). The presence of clouds is apparent by the strong signal in the aerosol channel with an attenuated signal at higher altitudes in the molecular channel.

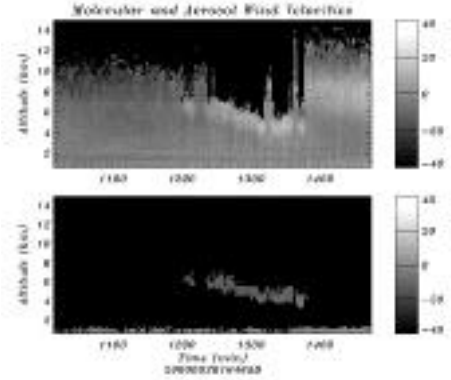

Figure 13: Wind velocities measured from the molecular and aerosol channels. These are a 1 minute integration time with a vertical resolution of .25 km below 3 km, and 1 km above 3km.

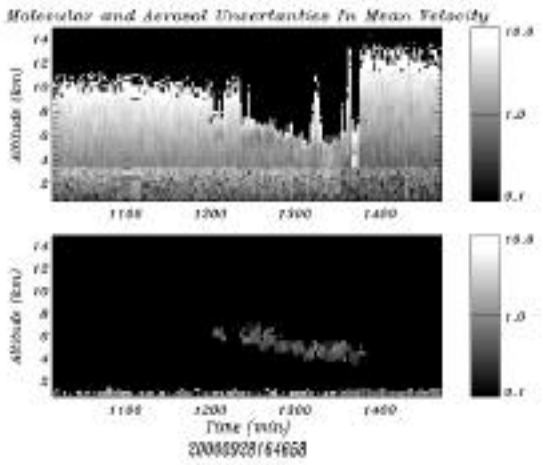

Figure 14: These uncertainties are standard deviations of the data points that were averaged in order to fit the data onto the grid that all instruments used (the same as in figure 12).

LOS wind velocities in New Hampshire, averaged over time, are shown below. The GroundWinds data can be compared to radiosonde data that are also plotted.

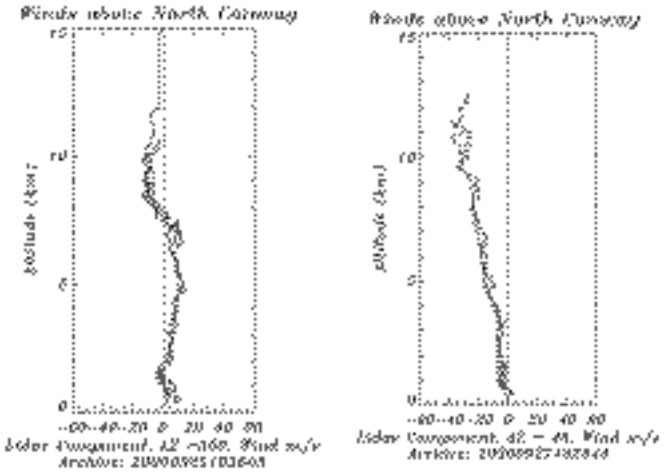

Figure 15: Two plots showing altitude profiles in the azimuth direction that GroundWinds was looking. The aerosol channel is shown via a square, and the molecular channel is shown with an asterisk. The radiosondes is the solid line. Note that on the 25th aerosol measurements were made from a thin cloud between 6 and 9 km..

Turbulence spectra are directly measured with the lidar using the time history of line-of-sight velocity at each elevation. Turbulence is a phenomenon with an important high frequency component. In order to capture a significant portion of the high frequency spectrum, the temporal resolution must be maximized, which requires minimizing the integration time during data collection. Experience with the sister facility in New Hampshire has shown that an integration time of 1 second, the shortest value that the instrument can achieve is adequate for extracting reliable turbulence spectra. At the higher elevations, this choice of integration time can result in a weak signal, sometimes dominated by noise.

A small number of isolated data points have unrealistic values sufficiently large to cause a significant numerical error when determining the spectra. For this reason, the unrealistic points are first removed. The unreliable data is removed with three filters; the first filter makes use of the recorded spectral fringe shape, and discards data whose correlation with a reference signal has a correlation coefficient less than 0.75. The second filter deletes velocities with an unrealistic magnitude; for the present results, velocities greater than 300 meters per second were discarded. The last filter assumes the time series to have a Gaussian distribution (only briefly, for filtering purposes), and deletes data points that lie outside three standard deviations. The Lomb-Scargle algorithm is used to determine the spectra. The Lomb-Scargle algorithm determines the spectra for time series with irregularly spaced data. An example of time series determined with the one-second integration time taken at the GroundWinds sister facility in New Hampshire are shown in figure 1. The associated spectrum is shown in figure 2, determined using the Lomb-Scargle technique.

The variability of the velocity measurement that results in the spectrum in figure 4 is due to a variety of effects that are classified into two types; atmospheric motion and noise. Atmospheric motion can take a vast variety of forms, including internal waves, shear flows, and many other coherent motions. In addition to the coherent flow is the incoherent motion, or turbulence. The high frequency end of the turbulence spectrum is generally proportional to $k^{-5/3}$. This interval of the spectrum is called the `inertial range'. The presence of this region of the $k^{-5/3}$ behavior is used to estimate the magnitude of the turbulence and noise separately. The magnitude of the turbulence is determined by fitting a $k^{-5/3}$ curve to the spectra, and calculating the coefficient. The coefficient is used to determine the velocity turbulence parameter c_V^2. Details can be found in Dors, et al. Note in figure 2 the curve fitted to the spectra. The slope of this curve on a logscale for the low frequency end is $k^{-5/3}$, and the position of this part of the curve determines the magnitude of the turbulence at this elevation.

The error generally increases with elevation. Most of this increase in error is due to the weakening of the backscattered light as the distance from the detector increases. As the noise level increases, the signal-to-noise ratio decreases, and the ability to extract turbulence levels is compromised. Furthermore, turbulence can be very weak at some elevations, even at low elevations where a strong signal is expected, and can again be difficult to extract. A measure of confidence in the turbulence estimates is obtained by creating a sequence of artificial time series with the same statistics as the original time series. The artificial turbulence in these artificial time series is used to estimate the confidence in the actual turbulence measurement.

A recent campaign (see Dors, et al.) compared the turbulence results of the lidar with a thermosonde measurement of c_T^2, the temperature turbulence parameter. The two measurements use different measures; the lidar uses velocity and the thermosonde uses temperature. These two measurements are independent in general. Despite this difference, The results showed excellent agreement in regions where the lidar data had acceptable confidence levels, despite this difference. This indicates that atmospheric turbulence usually has both a velocity and temperature signature, and `seeing' estimates can possibly be made with measures of velocity turbulence. There was one thin region where the two measurements resulted in drastically different estimates of turbulence dissipation. This region apparently corresponded to a well-mixed layer, where turbulence models used in the dissipation estimate are not reliable.

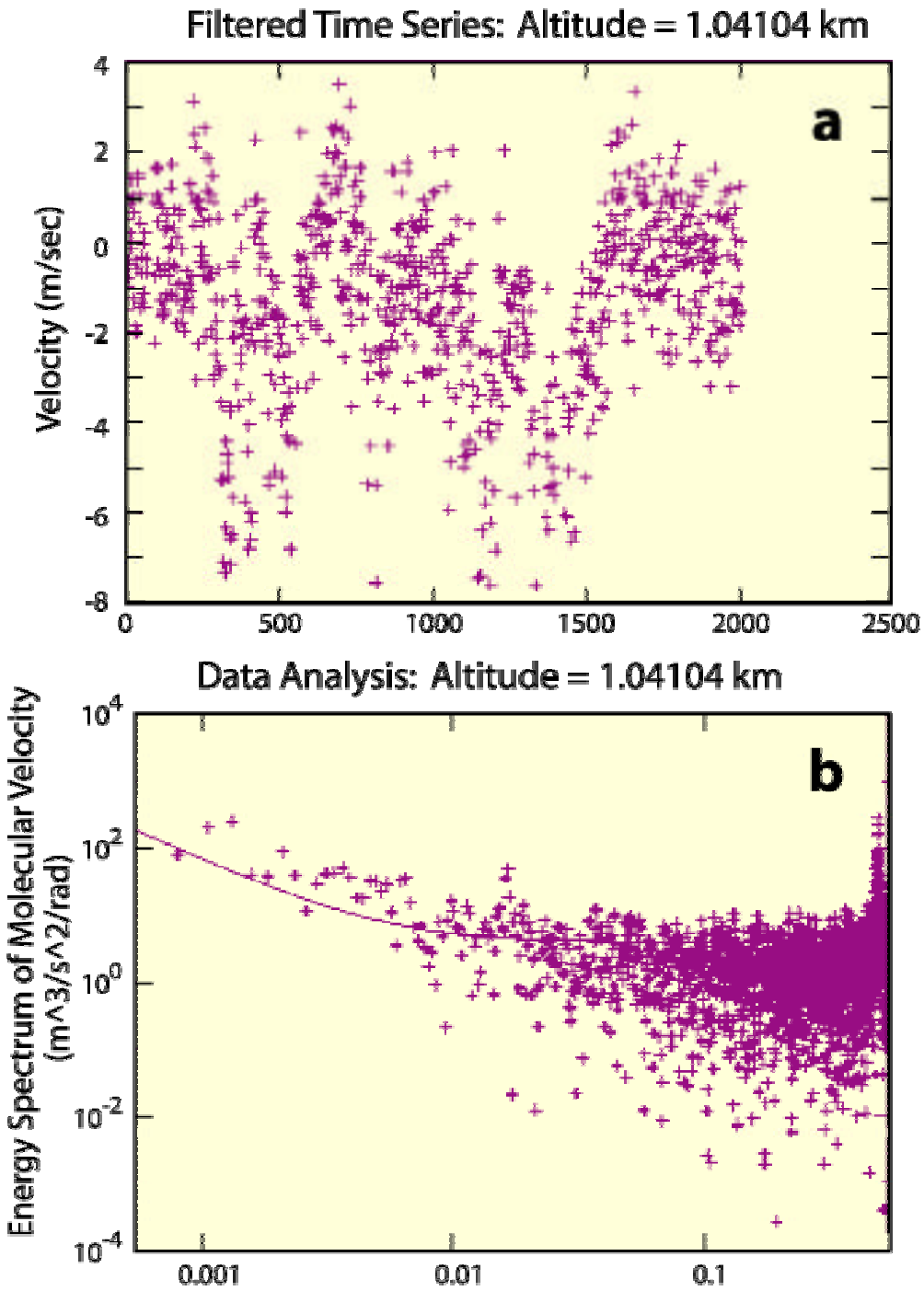

Fig. 16 Top: Time history of line-of-sight velocity measured by the lidar at an elevation of 1.04 km. Bottom: Spectrum of line-of-sight velocity measured by the lidar at an elevation of 1.04 km. The solid line is the curve fit for homogenous turbulence, has a slope of -2/3 at the low frequency end, an is used to extract turbulence amplitudes.

4. APPLICATIONS FOR MAUNA KEA

Data from the Mauna Loa lidar are being used in a custom forecast project, the Mauna Kea Weather Center (see http://hokukea.soest.hawaii.edu), which provides operational support for the world-class group of astronomical observatories on nearby Mauna Kea (Businger et al. 2002). The lidar data will be used to help prepare wind and turbulence forecasts for the summit of Mauna Kea and as input for an operational mesoscale numerical weather prediction model (MM5). Clear-air turbulence in both the free atmosphere and in the summit boundary layer causes phase distortions to incoming electromagnetic wave fronts, resulting in motion, intensity fluctuations (scintillation), and blurring of images obtained by ground-based telescopes. Astronomical parameters that quantify these effects are generically referred to as *seeing*. Seeing improves or degrades with changes in the vertical location and strength of turbulence as quantified by profiles of the refractive index structure function C_n^2 (Nastrom and Eaton 1993). C_n^2 fluctuations usually occur at scales that are too small for routine direct measurement, but they can be parameterized from vertical gradients in wind, temperature, and moisture in our MM5 runs. Seeing at a particular wavelength is then calculated by vertically integrating the C_n^2 profile (Fig. 17). Since seeing at Mauna Kea varies significantly from one night to the next, or even within one night, as a result of changing synoptic and mesoscale flow patterns, accurate seeing forecasts from MM5 enable telescopes to take best advantage of conditions that are favorable for a particular type of observation. LIDAR wind profiles represent an important data resource for MM5 model input and verification.

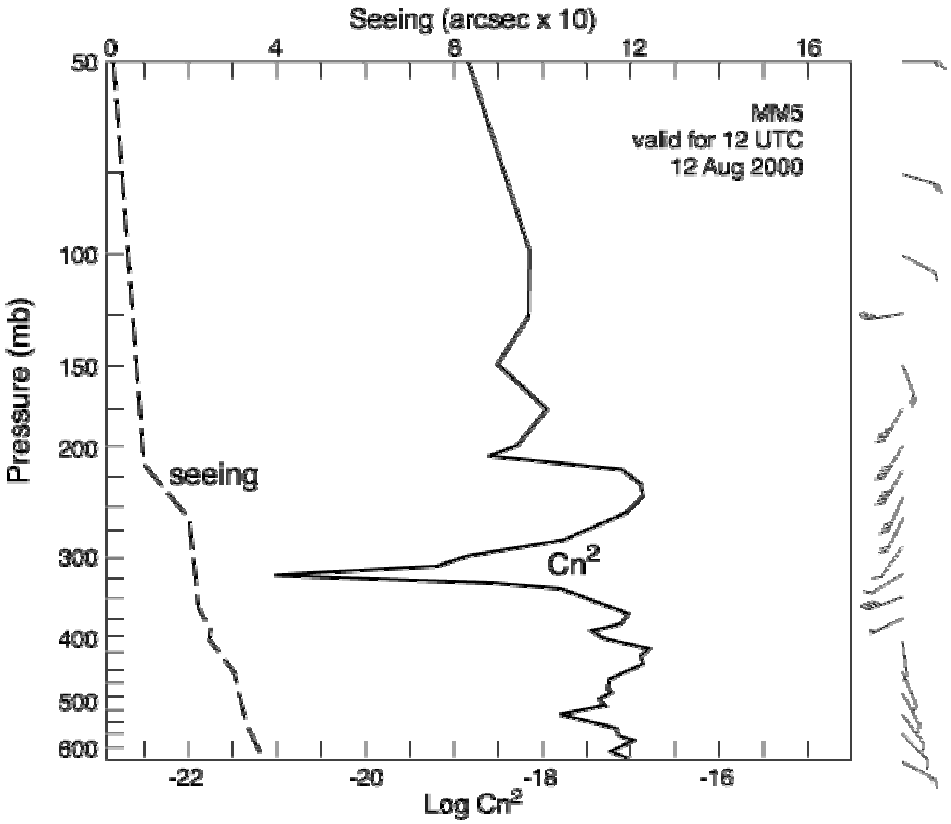

Fig. 17 C_n^2 and seeing profiles output from MM5 for a day with very good seeing quality, valid at 12 UTC on 2 August 2000. Wind barbs on right have the usual convention. After Businger et al. 2001.

Although a primary interest of the astronomical community are forecasts that predict atmospheric variability during relatively fair weather conditions, the observatories and Hawaiian society in general are vulnerable to significant hazards associated with organized storm systems (e.g., heavy rainfall, blizzard conditions, and high winds). The Mauna Kea Weather Center faces special challenges in forecasting these storms as a consequence of a serious lack of observational data over the central Pacific region and the pronounced impact of large mountains on the atmosphere. The promise of global upper level winds from the coherent lidar represents an important new data source for weather predictions. Some

examples are briefly outlined here.

Kona lows are subtropical cyclones that occur during the cool season in the north central Pacific. The Hawaiian adjective, "kona", meaning leeward, is used to describe winds with a southerly component that replace the usually persistent trade wind regime. Historically kona lows have produced a variety of weather related hazards including heavy rains, hailstorms, flash floods, landslides, high winds, large surf and swell, waterspouts, and severe thunderstorms (e.g., Businger et al. 1998). The importance of upper-tropospheric dynamics (winds) in the development of kona lows in the central Pacific has been recently documented (Fig. 18)(Morrison and Businger 2001).

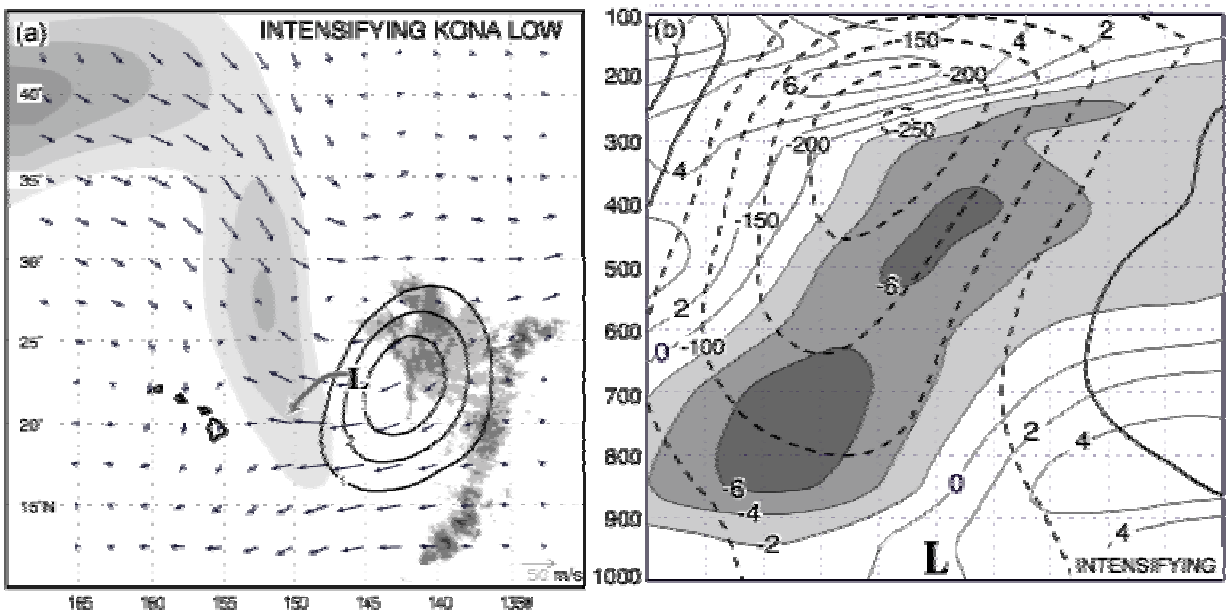

Fig. 18 (a) Analysis of 250-mb isotachs (shaded every 10 m s-1 greater than 50 m s^{-1}), divergence at 250 mb (solid and short dash, every 0.5 x 10-5 s^{-1}), ageostrophic wind (vectors, m s^{-1}), and IR satellite temperature (shading every 8˚C starting at -40˚C) for the period of most rapid deepening of a kona low. L indicates the position of the observed surface low, and the large arrow indicates the low's track to the next stage. (b) Cross section of height anomalies (bold dashed lines, m) and temperature anomalies (light lines and shaded regions, ˚C). The L indicates the reanalysis position of the surface low.

Between August of 1964 and December of 1994, 24 damaging trade wind events in Hawaii resulted in 17 deaths (16 at sea), 6 injuries and millions of dollars in damage. A case study and composite analysis show that the source of the enhanced surface winds is an enhanced pressure gradient over the Hawaiian Islands resulting from a strong surface high located ~1600 km north of Hawaii. Damaging downslope winds associated with strong surface highs near Hawaii have been linked to 250-mb jet streaks (Mello 2001). Composite analysis of 31 strong trade wind events at Lihue, Kauai, shows that the Hawaiian high initially forms as a warm core high close to Japan in the convergent right front quadrant of a 250-mb jet streak two days before the onset of the strongest winds (Fig. 19).

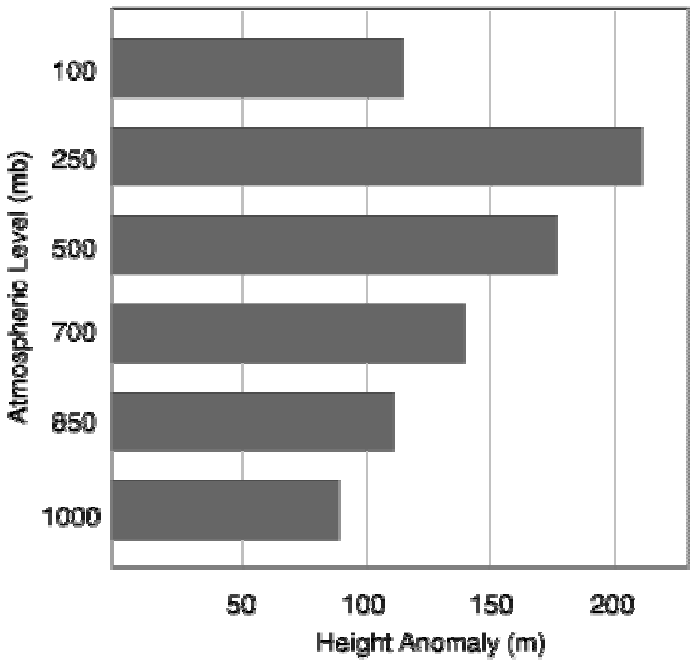

Fig. 19 The composite magnitude of height anomalies as a function of elevation in the troposphere for 31 damaging tradewind days

Finally, it is known that tropical cyclones track with deep tropospheric environmental flows that are very difficult to measure in the absence of reconnaissance aircraft. For these multiple reasons the potential of deriving global tropospheric winds in clear air through use of a space-based lidar system represents a significant advance in data coverage for large ocean areas of the globe that are now poorly sampled through radiosondes.

5. CONCLUSIONS

A coherent lidar has recently been commissioned at the GroundsWinds Obervatory located on the slope of Mauna Loa on the island of Hawaii. The new lidar can measure altitude resolved line-of-sight wind velocities, turbulence power spectra, aerosol content and faint cirrus clouds among other things of interest to astronomers. The lidar observatory employs spectral line profiling of incoherent backscattered 355 nm laser light. Very rapid measurement of the Doppler shift (400 ns resolution) is accomplished by feeding the returned laser light into a combination of two Fabry-Perot etalons and collapsing the interference fringes into a 1-dimensional interference pattern using a conical optic. This allows the system to get the maximum signal to noise ratio and best vertical resolution given the performance of the CCD. Each measurement takes 10 s. The molecular return is strong up to 15-km altitude. Data from the incoherent lidar are used in a custom forecasting project, the Mauna Kea Weather Center, which provides operational support for the world-class group of astronomical observatories located on the summit of Mauna Kea. The lidar data are used to help prepare wind and turbulence nowcasts/forecasts for the summit of Mauna Kea (~4000 m) and as input for an operational mesoscale numerical weather prediction model (MM5). Lidar wind profiles represent an important data resource for nowcasting seeing, input for MM5 initial conditions and algorithm refinement, and for forecast verification.

6. ACKNOWLEDGEMENTS

The authors would like to thank the staff of Michigan Aerospace Corporation, as well as the staff of the University of New Hampshire and the Mount Washington Observatory. The efforts of Lynn Rosentrater, Michelle Day, and Ken Rancourt were particularly critical to the successful outcome of the validation campaign. Additionally, the investment made in this project by our suppliers made a difference between success and failure. We would like to thank Continuum, Torus Technologies, PixelVision and Process Results for their contributions to the development of this technology. This research is supported by NOAA under grant NA17EC1105.

7. REFERENCES

Businger, S., T. Birchard, Jr., K.R. Kodama, P.A. Jendrowski, and J-J Wang, 1998: A bow echo and severe weather associated with a Kona Low in Hawaii. *Wea. and Forecasting*, **13**, 576-591.

Businger, S., R. McLaren, R. Ogasawara, D. Simons, and R.J. Wainscoat, 2001: Starcasting. *Bull. Amer. Met. Soc*., **83**, 858–871.

Hays, P.B., 1990. Circle to line interferometer optical system. *Applied Optics, us.* 29(1 April):1482-1489.

Hays, P.B., et al 1993. The High-Resolution Doppler Imager on the Upper Atmosphere Research Satellite. *Journal of Geophysical Research* Vol.98 No. D6:10,713-10,723.

Jacquinot, P. 1954. The Luminosity of Spectrometers with Prisms, Gratings or Fabry-Perot Etalons. *American Journal Optical Society*. 44:761-765.

Killeen, Timothy L. and Hays, P.B. 1984. Doppler line profile analysis for a multichannel Fabry-Perot interferometer. *Applied Optics, us.* 23(15 February):612-620.

Mello, C. 1999: Damaging Trade Winds in Hawaii. MS Thesis. Dept. of Meteor., Univ. of Hawaii, 2525 Correa Rd. Honolulu, HI 96822, 51 pp.

Morrison, I. and S. Businger, 2001: The synoptic structure and evolution of a kona low. *Wea. and Forecasting*, **16**, 81-98.

Nastrom, G. D., and F. D. Eaton, 1993: The coupling of gravity waves and turbulence at White Sands, New Mexico, from VHF radar observations. *J. Appl. Meteor*., **32**, 81-87.Dors, I, McHugh, J, Jumper G, Roadcap, J, et al. Turbulence measurements using incoherent lidar, and comparison with thermosonde measurements. Submitted.

Rees, David and McDermid, I Stuart. 1990. Doppler lidar atmospheric wind sensor: Reevaluation of a 355-nm incoherent Doppler lidar. *Applied Optics, us.* 29(1 October):4133-4144.

Wang, C.C. et al. 1994. University of Michigan Ground-Based Circle-to-Line Fabry-Perot Interferometer and its Applications in Mesosphere and Lower Thermosphere Dynamics Studies. *Optical and Spectroscopic Techniques andInstrumentation for Atmospheric and Space Research, San Diego, SPIE Proceedings,* 2266:133-142.